



LAWRENCE  
LIVERMORE  
NATIONAL  
LABORATORY

# Ground-Motion Simulations of Scenario Earthquakes on the Hayward Fault

B. Aagaard, R. Graves, S. Larsen, S. Ma, A. Rodgers,  
D. Ponce, D. Schwartz, R. Simpson, R. Graymer

March 10, 2009

Third Conference on Earthquake Hazards in the Eastern San  
Francisco Bay Area  
Hayward, CA, United States  
October 22, 2008 through October 24, 2008

## **Disclaimer**

---

This document was prepared as an account of work sponsored by an agency of the United States government. Neither the United States government nor Lawrence Livermore National Security, LLC, nor any of their employees makes any warranty, expressed or implied, or assumes any legal liability or responsibility for the accuracy, completeness, or usefulness of any information, apparatus, product, or process disclosed, or represents that its use would not infringe privately owned rights. Reference herein to any specific commercial product, process, or service by trade name, trademark, manufacturer, or otherwise does not necessarily constitute or imply its endorsement, recommendation, or favoring by the United States government or Lawrence Livermore National Security, LLC. The views and opinions of authors expressed herein do not necessarily state or reflect those of the United States government or Lawrence Livermore National Security, LLC, and shall not be used for advertising or product endorsement purposes.

# Ground-Motion Simulations of Scenario Earthquakes on the Hayward Fault

by

Brad T. Aagaard<sup>1</sup>, Robert W. Graves<sup>2</sup>, Shawn C. Larsen<sup>3</sup>, Shuo Ma<sup>4</sup>, Arthur Rodgers<sup>5</sup>, David A. Ponce<sup>6</sup>, David Schwartz<sup>7</sup>, Robert W. Simpson<sup>8</sup>, and Russell W. Graymer<sup>9</sup>

## ABSTRACT

We compute ground motions in the San Francisco Bay area for 35 Mw 6.7–7.2 scenario earthquake ruptures involving the Hayward fault. The modeled scenarios vary in rupture length, hypocenter, slip distribution, rupture speed, and rise time. This collaborative effort involves five modeling groups, using different wave propagation codes and domains of various sizes and resolutions, computing long-period ( $T > 1\text{--}2$  s) or broadband ( $T > 0.1$  s) synthetic ground motions for overlapping subsets of the suite of scenarios. The simulations incorporate 3-D geologic structure and illustrate the dramatic increase in intensity of shaking for Mw 7.05 ruptures of the entire Hayward fault compared with Mw 6.76 ruptures of the southern two-thirds of the fault. The area subjected to shaking stronger than MMI VII increases from about 10% of the San Francisco Bay urban area in the Mw 6.76 events to more than 40% of the urban area for the Mw 7.05 events. Similarly, combined rupture of the Hayward and Rodgers Creek faults in a Mw 7.2 event extends shaking stronger than MMI VII to nearly 50% of the urban area. For a given rupture length, the synthetic ground motions exhibit the greatest sensitivity to the slip distribution and location inside or near the edge of sedimentary basins. The hypocenter also exerts a strong influence on the amplitude of the shaking due to rupture directivity. The synthetic waveforms exhibit a weaker sensitivity to the rupture speed and are relatively insensitive to the rise time. The ground motions from the simulations are generally consistent with Next Generation Attenuation ground-motion prediction models but contain long-period effects, such as rupture directivity and amplification in shallow sedimentary basins that are not fully captured by the ground-motion prediction models.

<sup>1</sup>Brad Aagaard, U.S. Geological Survey, MS977, 345 Middlefield Rd, Menlo Park, CA 94025, baagaard@usgs.gov

<sup>2</sup>Robert Graves, URS Corporation, 566 El Dorado St., Pasadena, CA 91101, robert\_graves@urscorp.com

<sup>3</sup>Shawn Larsen, Lawrence Livermore National Laboratory, Box 808, L-103, Livermore, CA 94551-0808, larsen8@llnl.gov

<sup>4</sup>Shuo Ma, Dept. of Geol. Sciences, San Diego State University, 5500 Campanile Dr., San Diego, CA 92182-1020, sma@geology.sdsu.edu

<sup>5</sup>Arthur Rodgers, Lawrence Livermore National Laboratory, Box 808, L-205, Livermore, CA 94551-0808, rodders7@llnl.gov

<sup>6</sup>David Ponce, U.S. Geological Survey, MS989, 345 Middlefield Rd, Menlo Park, CA 94025, ponce@usgs.gov

<sup>7</sup>David Schwartz, U.S. Geological Survey, MS977, 345 Middlefield Rd, Menlo Park, CA 94025, dschwartz@usgs.gov

<sup>8</sup>Robert Simpson, U.S. Geological Survey, MS977, 345 Middlefield Rd, Menlo Park, CA 94025, simpson@usgs.gov

<sup>9</sup>Russell Graymer, U.S. Geological Survey, MS975, 345 Middlefield Rd, Menlo Park, CA 94025, rgraymer@usgs.gov

## OBJECTIVES

22 The Uniform California Earthquake Rupture Forecast released in 2008 assigned a probability of 31% for a magnitude  
23 6.7 or larger event occurring on the Hayward-Rodgers Creek fault system in the next 30 years (Working Group on California  
24 Earthquake Probabilities, 2008). The previous large earthquake on the Hayward fault was a magnitude 6.8 event rupturing  
25 the southern two-thirds of the fault in 1868 (Yu and Segall, 1996; Bakun, 1999). The focus of this study is to characterize  
26 the ground shaking across a suite of scenarios spanning a range of possible events for the next large earthquake involving  
27 the Hayward fault. We develop kinematic rupture models based on previous probability forecasts (e.g., Working Group on  
28 California Earthquake Probabilities (2003) and Working Group on California Earthquake Probabilities (2008)) and geophysical  
29 data while attempting to make the resulting ground motions consistent with the Next Generation Attenuation models (e.g.,  
30 Boore and Aktinson (2008)). In this paper we present an overview of the modeling results; a more thorough discussion of the  
31 results is available in Aagaard *et al.* (in prep.) and Aagaard *et al.* (in prep.).

## EARTHQUAKE SCENARIOS

32 The suite of earthquake scenarios spans a large range of parameters through variability in rupture length, hypocenter,  
33 slip distribution, rupture speed, and rise time. The five rupture lengths (Figure 1) include (1) the southern two-thirds of the  
34 Hayward fault (Hayward South), (2) the entire Hayward fault (Hayward South + North), (3) a portion of the Central Calaveras  
35 and the southern two-thirds of the Hayward fault (Central Calaveras + Hayward South), (4) the northern portion of the Hayward  
36 fault and the Rodgers Creek fault (Hayward North + Rodgers Creek), and (5) the Hayward fault and the Rodgers Creek fault  
37 (Hayward South + North + Rodgers Creek). These rupture lengths closely follow those from the Working Group on California  
38 Earthquake Probabilities (2003) with the addition of the Central Calaveras + Hayward South rupture, which is based on recent  
39 seismic, geologic, and geophysical evidence that at depth the Hayward fault extends south to the Central Calaveras fault as a  
40 relatively smooth, continuous structure (Manaker *et al.*, 2005; Graymer *et al.*, 2007). For each of the first three rupture lengths  
41 (Hayward South, Hayward South + North, and Central Calaveras + Hayward South), we consider three hypocenters yielding  
42 north-to-south rupture, bilateral rupture, and south-to-north rupture. These hypocenters were selected based on the empirical  
43 results of Mai *et al.* (2005) that identified a preference for hypocenters in strike-slip ruptures to sit in deeper sections of the  
44 fault. We also selected random realizations of slip (discussed in the following paragraphs) consistent with these hypocenters  
45 lying near regions with large slip. For the ruptures involving both the Hayward and Rodgers Creek faults we consider only a  
46 single hypocenter under San Pablo Bay, because ruptures have great difficulty jumping across 5-km step-overs between strike-  
47 slip faults (Harris and Day, 1993), like the one between the Hayward and Rodgers Creek faults. Ruptures may nucleate on  
48 secondary structures in such step-overs and subsequently spread onto adjacent faults. In this way the hypocenter under San  
49 Pablo Bay is analogous to the 1906 earthquake, which nucleated in a geometrically complex region offshore of San Francisco  
50 (Lomax, 2005; Lomax, 2008), and the 1995 Kobe earthquake, which nucleated in a geometrically complex region at the

51 intersection of the Nojima fault and the Suma and Suwayama fault (Zhao *et al.*, 1996).

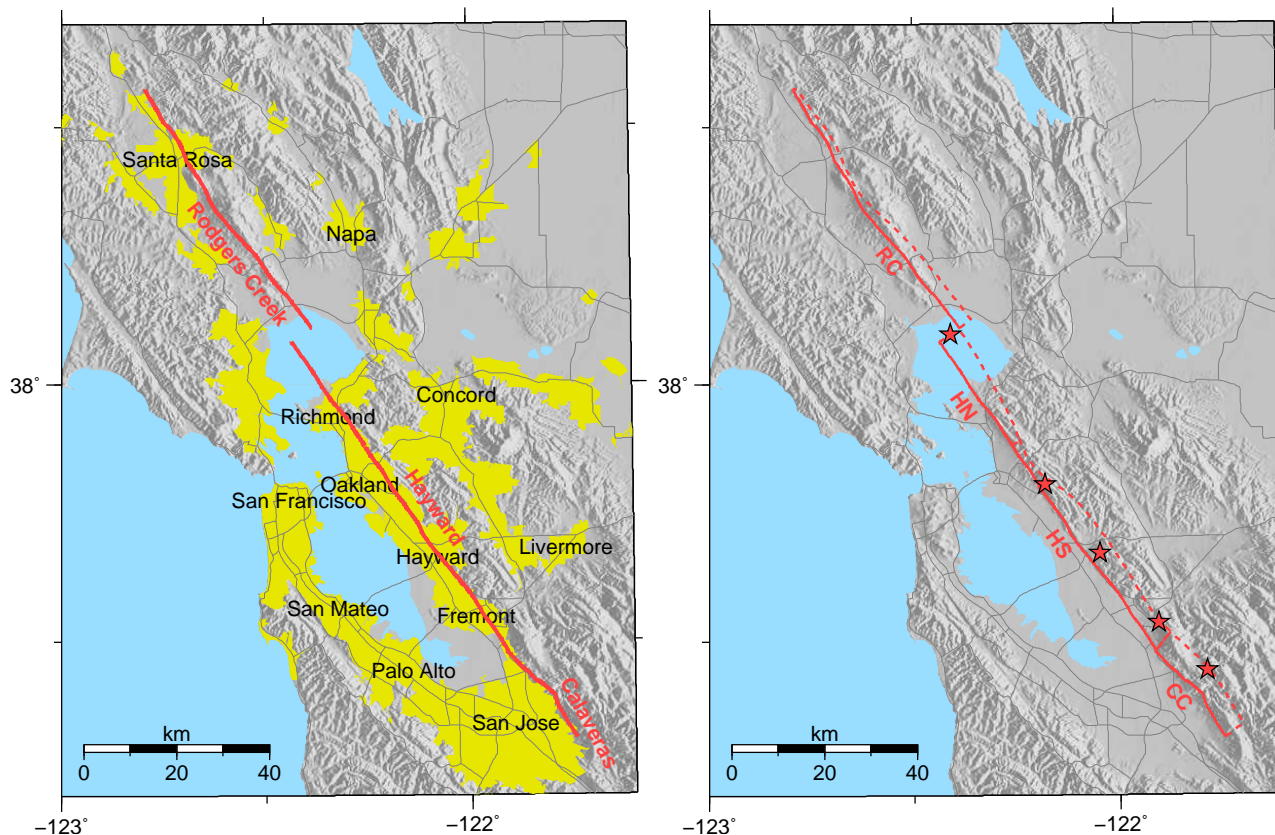


Figure 1. The left panel shows a map of the urban area (yellow shaded region) and the extent of rupture on the surface traces (red lines) of the scenarios for the Hayward, Rodgers Creek, and Calaveras faults. The right panel shows the four rupture segments (surfaces traces in solid red lines and down-dip extent of rupture in dashed red lines) which are combined into the five rupture lengths. The epicenters (stars) are offset from the surface trace due to the 3D geometry of the fault surface. The rupture segments include the Central Calaveras (CC), Hayward South (HS), Hayward North (HN), and Rodgers Creek (RC).

52 The slip distribution in each scenario is a combination of a deterministic long length-scale distribution (nominal or  
53 background slip at scales longer than 1/2 of the rupture length) and a stochastic short length-scale distribution (scales shorter  
54 than 1/2 of the rupture length). For each hypocenter we consider multiple realizations of the stochastic slip distributions. For  
55 the deterministic, background slip distribution, we account for the influence of creep on the coseismic rupture via two different  
56 approaches; both of these approaches use the creeping patches on the Hayward fault delineated by *Funning et al.* (2007). In the  
57 first set of slip distributions, we apply a slip-predictable approach (Shimazaki and Nakata, 1980) such that locked regions have  
58 a nominal slip equal to the product of the fault slip rate (9 mm/yr for the Hayward and Rodgers Creek faults (Working Group  
59 on California Earthquake Probabilities, 2003)) and the time since the most recent large event (140 years and about 230 years  
60 for the Hayward and Rodgers Creek faults, respectively (Working Group on California Earthquake Probabilities, 2003)). In the  
61 creeping patches, we reduce the slip relative to the locked patches by subtracting the creep rate from the fault slip rate before  
62 multiplying by the time since the most recent event, where we use the creep rate from *Funning et al.* (2007). For Hayward

63 South ruptures this yields Mw 6.84 events, compared to Mw 6.89 events if we neglect the influence of creep.

64 Because slip-predictable models often do a poor job of forecasting the amount of slip in earthquakes (Murray and  
65 Segall, 2002; Bakun *et al.*, 2005), we also consider an alternative approach for how creep may affect the coseismic slip distri-  
66 bution. In the second set of slip distributions, we assume that creeping areas progressively reduce coseismic slip as the rupture  
67 propagates into them and apply a vertical gradient of -0.1 m/km to the nominal background slip in the creeping patches de-  
68 lined by Funning *et al.* (2007). That is, the nominal slip at depth over the rupture area is uniform but tapers linearly at a  
69 constant rate (uniform vertical gradient) over the shallow, creeping portions of the fault. In this approach the background slip  
70 is not constrained to be related to the slip rate and time since the most recent event, so we constrain the average slip using the  
71 Hanks and Bakun (2008) magnitude-area relation. We account for creep in using the magnitude-area relation by replacing the  
72 rupture area with an effective rupture area (the area required to yield the same seismic potency with uniform slip) in our com-  
73 putation of the expected magnitude for a given rupture extent. This is similar to the reduced area factor, R, used by the Working  
74 Group on California Earthquake Probabilities (2003). For Hayward South ruptures this yields Mw 6.76 events, compared to  
75 Mw 6.89 events if we neglect the influence of creep.

76 For both sets of models, slip at shorter length scales (less than one-half of the rupture length) has a random phase with a  
77 wavenumber squared falloff based on Mai and Beroza (2002). The crossover between the deterministic nominal slip distribution  
78 and the stochastic slip distribution was set to minimize the bias in spectral accelerations of synthetic ground motions (that were  
79 computed with a simple 1-D seismic velocity structure) with respect to the Boore and Aktinson (2008) NGA ground-motion  
80 prediction model.

81 The kinematic rupture models include local variations in rupture speed and use a ray-tracing algorithm to propagate the  
82 rupture front over the fault surface. The rupture speed correlates with slip to promote variations in the direction of propagation  
83 and force the rupture to propagate around regions with very little slip. In the simulations discussed here, the rupture speed is  
84  $0.1 V_s$  (where  $V_s$  is the shear-wave speed) for zero slip and increases linearly to the limiting speed for mode-II rupture ( $0.92$   
85  $V_s$ ) at the average slip. The rupture speed remains  $0.92 V_s$  for regions with slip greater than the average slip. Due to the up-dip  
86 and down-dip propagation of the rupture over the fault surface, the average rupture speed over the length of the rupture tends to  
87 be about  $0.85 V_s$  or slightly slower than the limiting speed for mode-II rupture ( $0.92 V_s$ ). As part of our suite of 35 scenarios,  
88 we also consider ruptures with slower and faster rupture speeds as discussed in Aagaard *et al.* (in prep.).

89 Although we are not attempting to simulate the 1868 Hayward fault earthquake in detail (because little is known about  
90 its source parameters), a few of the scenarios are designed to have source parameters that might be similar to this event. The  
91 Hayward South scenarios are consistent with the rupture length (Yu and Segall, 1996; Bakun, 1999) and magnitude (Bakun,  
92 1999) of the 1868 earthquake. Boatwright and Bundock (2008) suggest that the north-south symmetry of the intensities is  
93 consistent with bilateral rupture compared with either predominantly north-to-south or south-to-north rupture. Our selection  
94 of three hypocenters permits further analysis to identify which rupture propagation pattern is most consistent with the shaking

95 intensities from the 1868 event.

## GROUND-MOTION MODELING

96 Five ground-motion modeling groups participated in the effort to simulate ground motions for the suite of 35 scenarios.  
97 These groups included (1) Aagaard with a finite-element code (Aagaard *et al.*, 2001) resolving periods greater than 2.0 s, (2)  
98 Graves with a finite-difference code (Graves, 1996; Day and Bradley, 2001; Graves, 2008) resolving periods greater than 1.0  
99 s and periods greater than 0.1 s using a hybrid approach (Graves and Pitarka, 2004), (3) Larsen with a finite-difference code  
100 (Larsen and Schultz, 1995) resolving periods greater than 1.0 s, (4) Ma with a finite-element code (Ma and Liu, 2006) resolving  
101 periods greater than 2.0 s, and (5) Rodgers with a finite-difference code (Nilsson *et al.*, 2007) resolving periods greater than 2.0  
102 s. Each group simulated a common subset of the scenarios to verify consistency of the results among the various groups and  
103 then explored a different subset of the parameter space spanned by the scenario suite. All of the simulations incorporate the  
104 3-D geologic structure as described by the USGS 3-D Geologic Model (Jachens *et al.*, 2006; Watt *et al.*, 2007) and the latest  
105 version (08.3.0) of the USGS Bay Area Velocity Model (Brocher *et al.*, 2006). The long-period simulations impose a minimum  
106 shear-wave speed of 500–750 m/s; Graves’s broadband simulations, on the other hand, account for local site effects based upon  
107 the shear-wave speed in the uppermost 30 m ( $V_{s30}$ ) as well as nonlinear soil response.

108 Figure 2 shows the Modified Mercalli Intensities (MMI) for Graves’s broadband ( $T > 0.1$  s) simulations of three Mw  
109 6.76 Hayward South ruptures with the simple slip-gradient approach that accounts for creep. MMI is computed from peak  
110 horizontal velocities (PGV) and peak horizontal accelerations (PGA) following the relation developed by Wald *et al.* (2005)  
111 for use in ShakeMap. The intensities from the broadband simulations tend to exceed the long-period simulations by about  
112 0.2–0.4 MMI units due to the inclusion of higher frequencies; nevertheless, the pattern of shaking is consistent across all of the  
113 modeling groups and the intensities among the long-period simulations agree quite well. The strike-slip rupture generates the  
114 highest intensities along the strike of the fault away from the epicenter, as a result of rupture directivity. A region of locally  
115 higher slip at the southern end of the rupture contributes to the strong intensities in that region. Although the perimeter of the  
116 San Francisco Bay contains very soft soils, the sediment cover is relatively thin compared to the east side of the Hayward fault  
117 along the northern portion of the rupture. This region is marked by deep, soft sediments, which causes the shaking intensities  
118 to be significantly higher east of the Hayward fault compared to west of the fault. Locally higher intensities are also present as  
119 a result of amplification due to sedimentary basins underneath Livermore, west and east of San Jose, and San Pablo Bay.

120 The shaking intensities increase significantly as the rupture length is extended north corresponding to rupture of the  
121 Hayward fault in a Mw 7.05 event. Figure 3 displays the Modified Mercalli Intensities for Graves’s broadband simulations of  
122 three Hayward South + North ruptures using the simple slip-gradient approach that accounts for creep. The area subjected to  
123 shaking stronger than MMI VII increases from about 10% of the San Francisco Bay urban area for the Mw 6.76 scenarios to  
124 more than 40% of the urban area for the Mw 7.05 scenarios. We attribute the stronger shaking to the combination of a greater

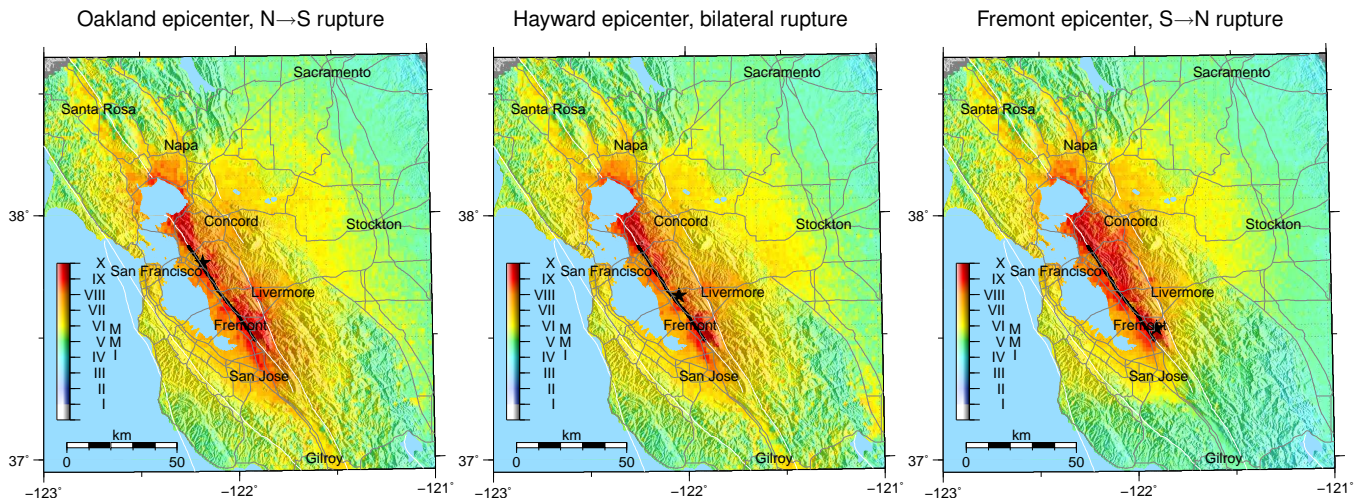


Figure 2. Maps of Modified Mercalli Intensity (MMI) for Graves's broadband simulation of three Mw 6.76 Hayward South ruptures that use the simple slip-gradient approach to account for creep. Rupture directivity (hypocenter), the slip distribution, and geologic structure all exhibit strong influences on the pattern of shaking.

125 rupture length (83 km compared with 54 km) and an increase in the average slip. The general pattern of shaking remains with  
 126 stronger motions along the strike of the fault away from the epicenter due to rupture directivity, stronger shaking along the  
 127 northern portion of the rupture east of the Hayward fault compared to west of the fault due to the contrast in rigidity (shear  
 128 modulus) across the fault, and local amplification in the sedimentary basins. Close to the rupture, we find variations in the  
 129 pattern of shaking as a result of using different random realizations of the slip in the stochastic portion of the slip distribution.

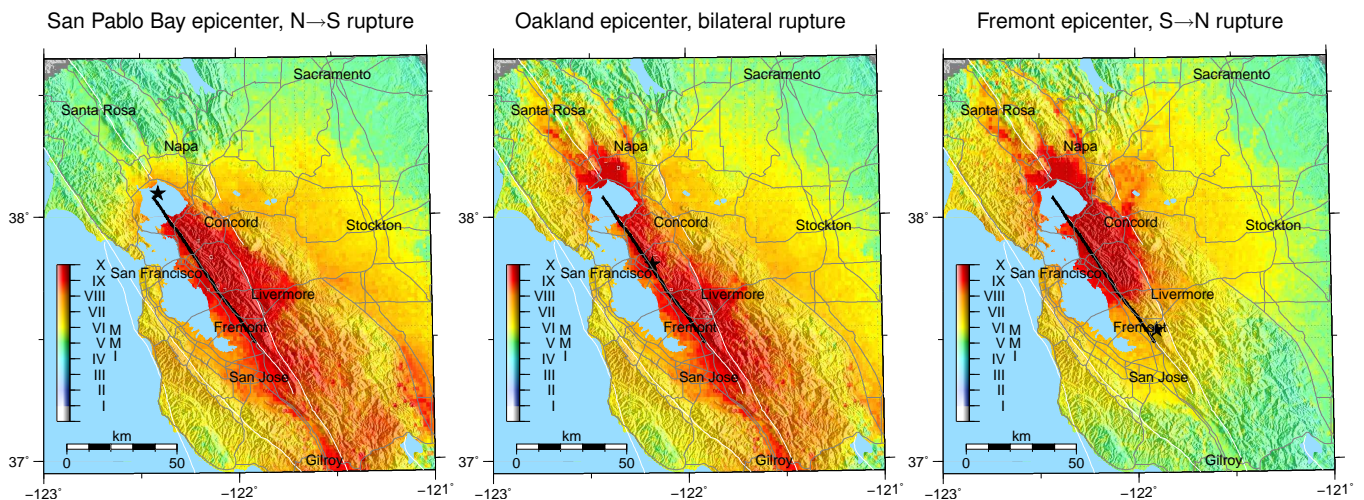


Figure 3. Maps of Modified Mercalli Intensity (MMI) for Graves's broadband simulations of three Mw 7.05 Hayward South+North ruptures that use the simple slip-gradient approach to account for creep. The longer rupture length and larger slip associated with the larger magnitude results in significantly stronger shaking in this scenario compared with the Mw 6.76 Hayward South ruptures shown in Figure 2.

130 Shifting the hypocenter near the north or south ends of rupture shifts the pattern of shaking. Hypocenters near the

131 southern ends of the ruptures increase the ground motions over the central and northern portions of the rupture and decrease the  
132 motions south of the epicenter. Likewise, hypocenters near the northern ends of the ruptures increase the ground motions over  
133 the central and southern portions of the rupture and decrease the motions north of the epicenter. This variation is consistent  
134 with the previous studies of rupture directivity (Somerville *et al.*, 1997; Aagaard *et al.*, 2001; Spudich and Chiou, 2008).

135 Across the suite of 35 scenarios, the synthetic ground motions exhibit the strongest sensitivity to the slip distribution  
136 and proximity to sedimentary basins. The hypocenter also exerts a strong influence on the amplitude of the shaking due to  
137 rupture directivity. Although not shown in this limited subset of the scenarios, the synthetic waveforms exhibit a weaker  
138 sensitivity to the rupture speed and are relatively insensitive to the rise time.

139 Figure 4 compares Modified Mercalli Intensity from Graves's broadband simulations of three Mw 6.76 Hayward  
140 South ruptures with the intensities of the 1868 earthquake compiled by Boatwright and Bundock (2008). The limited number of  
141 intensity observations (62) and unknown slip distribution for the 1868 earthquake limit the level of agreement, but the simulation  
142 with bilateral rupture produces intensities most consistent with those from the 1868 earthquake. However, all three Mw 6.76  
143 scenarios fit the 1868 intensities relative to the uncertainty in the slip distribution and our expectations based on our previous  
144 efforts to match MMI values for the Loma Prieta earthquake (Aagaard *et al.*, 2008b). The other scenarios from the suite of  
145 scenarios (not shown) exhibit significantly less consistency with the observed intensities from the 1868 earthquake, especially  
146 scenarios with larger magnitudes. Thus, the simulations support previous studies (Bakun, 1999) that assign a magnitude of  
147 about 6.8 to the 1868 earthquake.

148 The suite of scenarios also permits comparison of the motions calculated in 3-D models with ground-motion prediction  
149 relations, such as the Next Generation Attenuation (NGA) relations (Abrahamson and Silva, 2008; Boore and Aktinson, 2008;  
150 Campbell and Bozorgnia, 2008; Chiou and Youngs, 2008). In preliminary calculations (not shown here) we used the Boore  
151 and Aktinson (2008) ground-motion prediction model to calibrate the wavenumber at which we cross-over from the nominal,  
152 background slip distribution to the stochastic slip distribution. This calibration used a simple 1-D seismic velocity structure and  
153 focused on the mean residual, not the variance or spatial variation. Figure 5 compares spectral accelerations at periods of 0.3 s,  
154 1.0 s, and 3.0 s from Graves's broadband simulation of the Mw 6.76 Hayward South bilateral rupture (shown in Figure 2) with  
155 those predicted by the Boore and Aktinson (2008) NGA model. The variance is quite small at a period of 0.3 s and increases  
156 significantly at periods of 1.0 s and 3.0 s. The residuals for the other NGA models are similar in most cases. The mean residuals  
157 correspond to event terms in the ground-motion prediction models and express how the average ground motions from the 3-D  
158 simulations differ from the median of the ground motion prediction model for the specified earthquake magnitude. The mean  
159 residuals are generally less than about 25% across Graves's six broadband simulations and are well below the one standard  
160 deviation levels of the Boore and Aktinson (2008) ground-motion prediction equations, which range from about 35% to 50%  
161 over the period range of 0.3–3.0 s. This indicates that the ground motions from the 3-D simulations are, on average, consistent  
162 with the expected range of event-to-event variability observed in recorded earthquakes of the same magnitude.

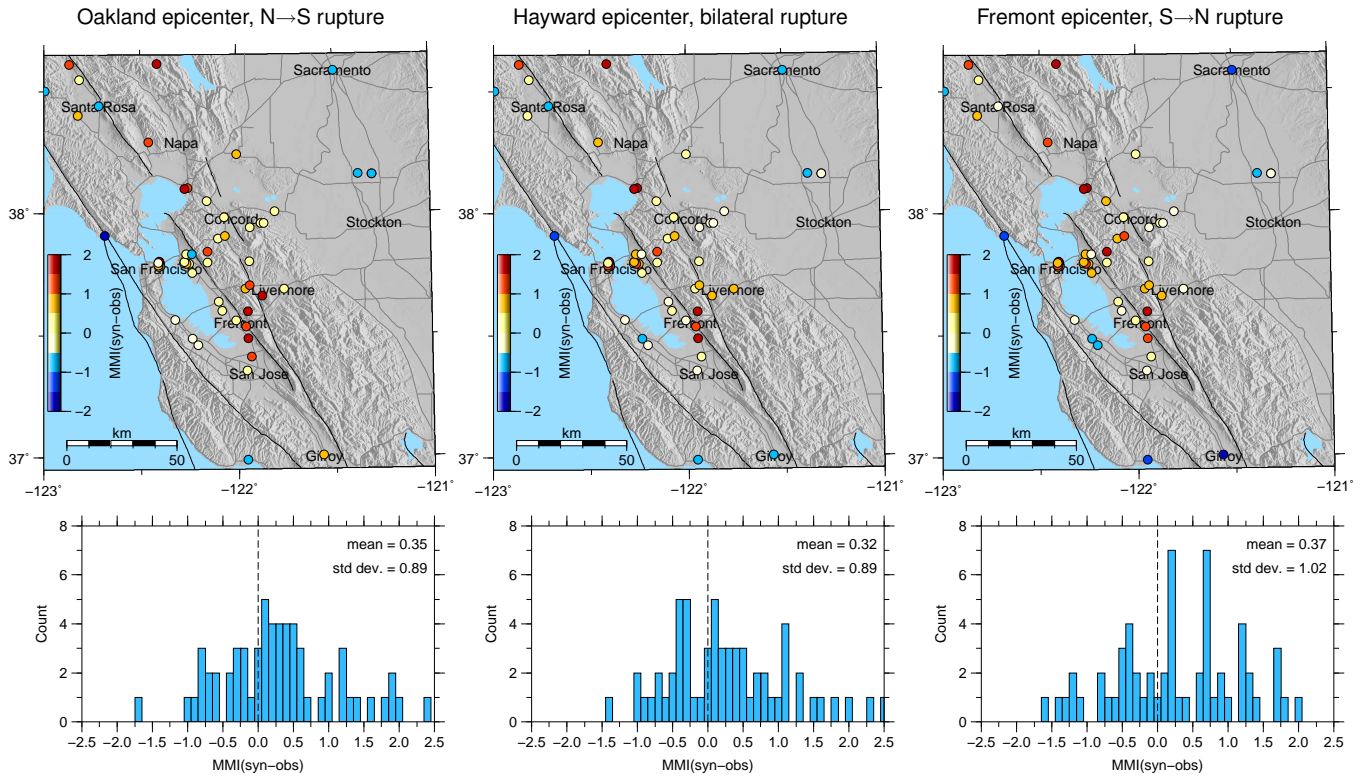


Figure 4. Maps (top) and histograms (bottom) showing comparison between Graves's broadband simulations of three Mw 6.76 Hayward South scenarios with different hypocenters and the Boatwright and Bundock intensities for the 1868 earthquake. The warmer and cooler colors indicate the simulations over-predict and under-predict the intensities, respectively. All three scenarios fit the 1868 intensities reasonably well with the bilateral rupture providing the best match to observed intensities.

163 The variances for the spectral accelerations at periods of 1.0 s and 3.0 s, on the other hand, are quite large. At  
 164 these periods the spectral accelerations from the 3-D simulations exceed the empirical relation in regions with strong forward  
 165 directivity and fall below the empirical relation in regions with backward directivity; consequently, the spectral accelerations at  
 166 1.0 and 3.0 s at most sites are highly sensitive to the hypocenter. Within sedimentary basins the spectral accelerations at 1.0 and  
 167 3.0 s consistently exceed the empirical predictions by a factor of up to 2 to 3. The NGA models account for basin amplification  
 168 either through Vs30 alone (Boore and Atkinson, 2008) or through a combination of Vs30 and a basin depth term (Abrahamson  
 169 and Silva, 2008; Campbell and Bozorgnia, 2008; Chiou and Youngs, 2008). However, most of the ground-motion data used to  
 170 constrain these models are from deep basins (e.g., the Los Angeles basin) or come from theoretical studies within deep basin  
 171 environments (Day *et al.*, 2008). The models also do not explicitly account for basin-edge effects or the coupling of directivity  
 172 and basin amplification. Most the basins within the greater San Francisco Bay area are relatively shallow (California Division  
 173 of Oil and Gas, 1982; McCulloch, 1987; Meltzer *et al.*, 1987; Stanley, 1985; Wentworth *et al.*, 1995; Parsons *et al.*, 2003;  
 174 Catchings *et al.*, 2004; Brocher, 2005; Catchings *et al.*, 2006) but have significant effects on the amplitude and duration of the  
 175 shaking (Frankel and Vidale, 1992; Hartzell *et al.*, 2006; McPhee *et al.*, 2007; Aagaard *et al.*, 2008b; Aagaard *et al.*, 2008a).  
 176 This suggests that refinement of the ground-motion prediction models may be required in order to adequately account for the  
 177 effects of amplification in shallow basins.

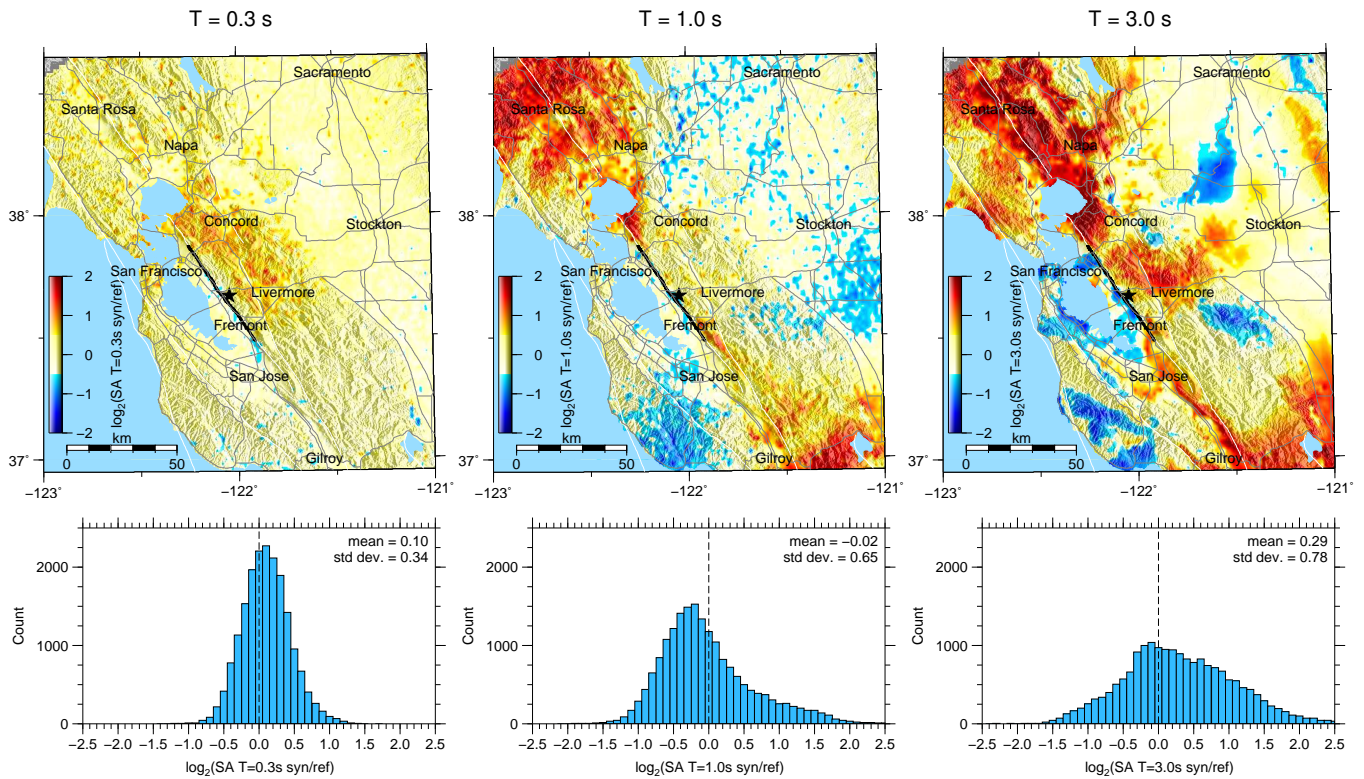


Figure 5. Maps (top) and histograms (bottom) of residuals in spectral acceleration at 0.3 s, 1.0 s, and 3.0 s for Graves's broadband simulations of the Mw 6.76 Hayward South bilateral rupture with respect to the Boore and Atkinson NGA model. The scale in the colorbar is  $\log_2$  so that the tickmarks of -2, -1, 0, 1, and 2 in the top panels correspond to differences of 1/4, 1/2, 1, 2, and 4, respectively. The mean residuals are close to zero, but the variance in the residuals increase with period because the NGA model fails to capture the effects of rupture directivity and amplification in shallow basins that are included in the simulations.

## CONCLUSIONS

178 This suite of simulations illustrates the seismic hazard posed by the Hayward fault to the San Francisco area. Economic  
 179 loss analyses performed by Zoback (in prep.) indicate that losses for our Mw 6.76 Hayward South earthquakes would be about  
 180 \$100 billion and reach about \$200 billion for our Mw 7.05 Hayward South + North earthquakes. Communities along the fault  
 181 rupture would be severely impacted. Furthermore, if the rupture is predominantly unilateral, the damage would be focused at  
 182 either the northern or southern end of the rupture. For example, a southern hypocenter would tend to focus damage towards the  
 183 northern end of the fault (including the cities of Oakland, Berkeley, and Richmond), and a northern hypocenter would focus  
 184 damage towards the the southern end of the fault (including the cities of San Jose and Fremont).

## ACKNOWLEDGMENTS

185 We thank Thomas Brocher, Ruth Harris, James Lienkaemper, and Paul Spudich for helpful discussions throughout  
 186 our modeling efforts. Reviews by David Boore and Paul Spudich led to improvements in the manuscript. Aagaard, Ponce,

187 Schwartz, Simpson, and Graymer were supported by the Earthquake Hazards Program of the U.S. Geological Survey. Graves  
188 was supported by funding from the Southern California Earthquake Center (SCEC) under NSF grants EAR-0623704 and OCI-  
189 0749313. Graves's simulations were run at the University of Southern California Center for High Performance Computing and  
190 Communications ([www.usc.edu/hpcc](http://www.usc.edu/hpcc)) under an agreement with the SCEC Community Modeling Environment project. Com-  
191 puting resources for Larsen's simulations were provided by the Department of Energy's Advanced Computational Technology  
192 Initiative. Ma was supported by funding from the USGS National Earthquake Hazards Reduction Program (award number  
193 08HQGR0013) and the Southern California Earthquake Center. Many of the figures were generated using Generic Mapping  
194 tools (Wessel and Smith, 1998) and the low-pass filtering of the waveforms was performed using SAC2000 (Goldstein *et al.*,  
195 2003). Prepared by LLNL under Contract DE-AC52-07NA27344.

## REFERENCES

- 196 Aagaard, B. T., T. M. Brocher, D. Dolenc, D. Dreger, R. W. Graves, S. Harmsen, S. Hartzell, S. Larsen, K. McCandless, S. Nilsson, N. A.  
197 Petersson, A. Rodgers, B. Sjögren, and M. L. Zoback, 2008a, Ground motion modeling of the 1906 San Francisco earthquake II: Ground  
198 motion estimates for the 1906 earthquake and scenario events, *Bulletin of the Seismological Society of America*, v. 98, no. 2, p. 1012–1046.
- 199 Aagaard, B. T., T. M. Brocher, D. Dolenc, D. Dreger, R. W. Graves, S. Harmsen, S. Hartzell, S. Larsen, and M. L. Zoback, 2008b, Ground motion  
200 modeling of the 1906 San Francisco earthquake I: Validation using the 1989 Loma Prieta earthquake, *Bulletin of the Seismological Society*  
201 *of America*, v. 98, no. 2, p. 989–1011.
- 202 Aagaard, B. T., R. W. Graves, S. Ma, S. C. Larsen, A. Rodgers, N. A. Petersson, R. C. Jachens, T. M. Brocher, R. W. Simpson, and D. Dreger,  
203 Ground motion modeling of Hayward fault scenario earthquakes II: Simulation of long-period and broadband ground motions, in preparation.
- 204 Aagaard, B. T., R. W. Graves, D. Schwartz, J. Linkaemper, D. A. Ponce, and R. W. Graymer, Ground motion modeling of Hayward fault scenario  
205 earthquakes I: Construction of the suite of scenarios, in preparation.
- 206 Aagaard, B. T., J. F. Hall, and T. H. Heaton, 2001, Characterization of near-source ground motions with earthquake simulations, *Earthquake*  
207 *Spectra*, v. 17, no. 2, p. 177–207.
- 208 Abrahamson, N. and W. Silva, 2008, Summary of the abrahamson & silva nga ground-motion relations, *Earthquake Spectra*, v. 24, no. 1,  
209 p. 67–97.
- 210 Bakun, W. H., 1999, Seismic activity of the San Francisco Bay region, *Bulletin of the Seismological Society of America*, v. 89, no. 3, p. 764–784.
- 211 Bakun, W. H., B. T. Aagaard, B. Dost, W. L. Ellsworth, J. L. Hardebeck, R. A. Harris, C. Ji, M. J. S. Johnston, J. Langbein, J. J. Lienkaemper,  
212 A. J. Michael, J. R. Murray, R. M. Nadeau, P. A. Reasenber, M. S. Reichle, E. A. Roeloffs, A. Shakal, R. W. Simpson, and F. Waldhauser,  
213 2005, Implications for prediction and hazard assessment from the 2004 Parkfield earthquake, *Nature*, v. 437, p. 969–974.
- 214 Boatwright, J. and H. Bundock, 2008, Modified Mercalli Intensity maps for the 1868 Hayward earthquake plotted in ShakeMap format, U.S.  
215 Geological Survey Open-File Report 2008-1121, <http://pubs.usgs.gov/of/2008/1121/> (last accessed 2/18/2009).
- 216 Boore, D. M. and G. M. Atkinson, 2008, Ground-motion prediction equations for the average horizontal component of PGA, PGV, and 5%-damped  
217 PSA at spectral periods between 0.01 s and 10.0 s, *Earthquake Spectra*, v. 24, no. 1, p. 99–138.
- 218 Brocher, T., B. Aagaard, R. Simpson, and R. Jachens, 2006, The new USGS 3D seismic velocity model for Northern California, *Seismological*  
219 *Research Letters*, v. 77, no. 2, p. 271, Abstract, 2006 SSA Annual Meeting.
- 220 Brocher, T. M., 2005, A regional view of urban sedimentary basins in Northern California based on oil industry compressional-wave velocity and  
221 density logs, *Bulletin of the Seismological Society of America*, v. 95, no. 6, p. 2093–2114.

222 California Division of Oil and Gas, 1982, Oil and gas prospect wells drilled in California through 1980, California Division of Oil, Gas, and  
223 Geothermal Resources Technical Report TR01, [http://www.consrv.ca.gov/DOG/pubs\\_stats/technical\\_reports.htm](http://www.consrv.ca.gov/DOG/pubs_stats/technical_reports.htm).

224 Campbell, K. W. and Y. Bozorgnia, 2008, Nga ground motion model for the geometric mean horizontal component of PGA, PGV, PGD and 5%  
225 damped linear elastic response spectra for periods ranging from 0.01 to 10 s, *Earthquake Spectra*, v. 24, no. 1, p. 139–171.

226 Catchings, R. D., M. R. Goldman, and G. Gandhok, 2006, Structure and velocities of the northeastern Santa Cruz Mountains and  
227 the western Santa Clara Valley, California, from the SCSI-LR seismic survey, U.S. Geological Survey Open-File Report 2006-1014,  
228 <http://pubs.usgs.gov/of/2006/1014/>.

229 Catchings, R. D., M. R. Goldman, C. E. Steedman, and G. Gandhok, 2004, Velocity models, first-arrival travel times, and geometries of 1991 and  
230 1993 USGS land-based controlled-source seismic investigations in the San Francisco Bay area, California: In-line shots, U.S. Geological  
231 Survey Open-File Report 2004-1423, <http://pubs.usgs.gov/of/2004/1423/>.

232 Chiou, B. S. and R. R. Youngs, 2008, An NGA model for the average horizontal component of peak ground motion and response spectra,  
233 *Earthquake Spectra*, v. 24, no. 1, p. 173–215.

234 Day, S. M. and C. R. Bradley, 2001, Memory-efficient simulation of anelastic wave propagation, *Bulletin of the Seismological Society of America*,  
235 v. 91, no. 3, p. 520–531.

236 Day, S. M., R. Graves, J. Bielak, D. Dreger, S. Larsen, K. B. Olsen, A. Pitarka, and L. Ramirez-Guzman, 2008, Model for basin effects on  
237 long-period response spectra in southern California, *Earthquake Spectra*, v. 24, no. 1, p. 257–277.

238 Frankel, A. and J. Vidale, 1992, A three-dimensional simulation of seismic waves in the Santa Clara Valley, California, from a Loma Prieta  
239 aftershock, *Bulletin of the Seismological Society of America*, v. 82, no. 5, p. 2045–2074.

240 Funning, G. J., R. Burgmann, A. Ferretti, and F. Novali, 2007, Asperities on the Hayward fault resolved by PS-InSAR, GPS and boundary element  
241 modeling, *EOS Trans.*, v. 88, no. 52, S23C-04.

242 Goldstein, P., M. Dodge, D. Firpo, and L. Minner, 2003, *The IASPEI International Handbook of Earthquake and Engineering Seismology*, Chapter  
243 SAC2000: Signal processing and analysis tools for seismologists and engineers, London: Academic Press.

244 Graves, R. W., 1996, Simulating seismic-wave propagation in 3-D elastic media using staggered-grid finite-differences, *Bulletin of the Seismo-*  
245 *logical Society of America*, v. 86, no. 4, p. 1091–1106.

246 Graves, R. W., 2008, The seismic response of the San Bernardino basin region during the 2001 Big Bear Lake earthquake, *Bulletin of the*  
247 *Seismological Society of America*, v. 98, no. 1, p. 241–252.

248 Graves, R. W. and A. Pitarka, 2004, Broadband time history simulation using a hybrid approach, In 13th World Conference on Earthquake  
249 Engineering Conference Proceedings, Vancouver, Canada, paper no. 1098.

250 Graymer, R. W., V. E. Langenheim, R. W. Simpson, R. C. Jachens, and D. A. Ponce, 2007, Relatively simple through-going fault planes at  
251 large-earthquake faults depth may be concealed by the surface complexity of strike-slip, In W. D. Cunningham and P. Mann (Eds.), *Tectonics*  
252 *of Strike-Slip Restraining and Releasing Bends*, Volume 290, pp. 189–201. London: Geological Society.

253 Hanks, T. C. and W. H. Bakun, 2008, M-logA observations for recent large earthquakes, *Bulletin of the Seismological Society of America*, v. 98,  
254 no. 1, p. 490–494.

255 Harris, R. A. and S. M. Day, 1993, Dynamics of fault interaction - parallel strike-slip faults, *Journal of Geophysical Research - Solid Earth*, v. 98,  
256 no. B3, p. 4461–4472.

257 Hartzell, S., S. Harmsen, R. A. Williams, D. Carver, A. Frankel, G. Choy, R. C. Jachens, T. M. Brocher, and C. M. Wentworth, 2006, Modeling and  
258 validation of a 3D velocity structure for the Santa Clara Valley, California, for seismic-wave simulations, *Bulletin of the Seismological Society*  
259 *of America*, v. 96, no. 5, p. 1851–1881.

260 Jachens, R., R. Simpson, R. Graymer, C. Wentworth, and T. Brocher, 2006, Three-dimensional geologic map of Northern and Central California:  
261 A basin model for supporting earthquake simulations and other predictive modeling, *Seismological Research Letters*, v. 77, no. 2, p. 270,  
262 Abstract, 2006 SSA Annual Meeting.

263 Larsen, S. and C. A. Schultz, 1995, *Elas3d: 2D/3D elastic finite-difference wave propagation code*, Lawrence Livermore National Laboratory  
264 Technical Report UCRL-MA-121792, 19 p.

265 Lomax, A., 2005, A reanalysis of the hypocentral location and related observations for the great 1906 California earthquake, *Bulletin of the*  
266 *Seismological Society of America*, v. 95, no. 3, p. 861–877.

267 Lomax, A., 2008, Location of the focus and tectonics of the focal region of the California earthquake of 18 April 1906, *Bulletin of the Seismological*  
268 *Society of America*, v. 98, no. 2, p. 846–860.

269 Ma, S. and P. Liu, 2006, Modeling of the perfectly matched layer absorbing boundaries and intrinsic attenuation in explicit finite-element methods,  
270 *Bulletin of the Seismological Society of America*, v. 96, no. 5, p. 1779–1794.

271 Mai, P. M. and G. C. Beroza, 2002, A spatial random field model to characterize complexity in earthquake slip, *Journal of Geophysical Research*  
272 - *Solid Earth*, v. 107, no. B11.

273 Mai, P. M., P. Spudich, and J. Boatwright, 2005, Hypocenter locations in finite-source rupture models, *Bulletin of the Seismological Society of*  
274 *America*, v. 95, no. 3, p. 965–980.

275 Manaker, D. M., A. J. Michael, and R. Burgmann, 2005, Subsurface structure and kinematics of the CalaverasHayward fault stepover from  
276 three-dimensional Vp and seismicity, San Francisco Bay region, California, *Bulletin of the Seismological Society of America*, v. 95, no. 2,  
277 p. 446–470.

278 McCulloch, D. S., 1987, *Geology and Resource Potential of the Continental Margin of Western North America and adjacent ocean basins-*  
279 *Beaufort Sea to Baja California*, Volume 6 of Circum-Pacific Council for Energy and Mineral Resources, Earth Science Series, Chapter  
280 *Regional geology and hydrocarbon potential of offshore Central California*, pp. 353–401. American Association of Petroleum Geologists.

281 McPhee, D. K., V. E. Langenheim, S. Hartzell, R. J. McLaughlin, B. T. Aagaard, R. C. Jachens, and C. McCabe, 2007, Basin structure beneath  
282 the Santa Rosa Plain, northern California: Implications for damage caused by the 1969 Santa Rosa and 1906 San Francisco earthquakes,  
283 *Bulletin of the Seismological Society of America*, v. 97, no. 5, p. 1449–1457.

284 Meltzer, A. S., A. R. Levander, and W. D. Mooney, 1987, Upper crustal structure, Livermore Valley and vicinity, California coast ranges, *Bulletin*  
285 *of the Seismological Society of America*, v. 77, no. 5, p. 1655–1673.

286 Murray, J. and P. Segall, 2002, Testing time-predictable earthquake recurrence by direct measurement of strain accumulation and release,  
287 *Nature*, v. 419, p. 287–291.

288 Nilsson, S., N. A. Petersson, B. Sjögreen, and H. O. Kreiss, 2007, Stable difference approximations for the elastic wave equation in second order  
289 formulation, *SIAM Journal on Numerical Analysis*, v. 45, no. 5, p. 1902–1936.

290 Parsons, T., R. Sliter, E. L. Geist, R. C. Jachens, B. E. Jaffe, A. Foxgrover, P. E. Hart, and J. McCarthy, 2003, Structure and mechanics of  
291 the Hayward-Rodgers Creek fault step-over, San Francisco Bay, California, *Bulletin of the Seismological Society of America*, v. 93, no. 5,  
292 p. 2187–2200.

293 Shimazaki, K. and T. Nakata, 1980, Time-predictable recurrence model for large earthquakes, *Geophysical Research Letters*, v. 7, no. 4, p. 279–  
294 282.

295 Somerville, P. G., N. F. Smith, R. W. Graves, and N. A. Abrahamson, 1997, Modification of empirical strong ground motion attenuation relations  
296 to include the amplitude and duration effects of rupture directivity, *Seismological Research Letters*, v. 68, no. 1, p. 199–222.

297 Spudich, P. and B. S. J. Chiou, 2008, Directivity in NGA earthquake ground motions: Analysis using isochrone theory, *Earthquake Spectra*, v. 24,  
298 no. 1, p. 279–298.

299 Stanley, R. G., 1985, Middle Tertiary sedimentation and tectonics of the La Honda basin, central California, U.S. Geological Survey Open-File  
300 Report 85-596, 263 p.

301 Wald, D., B. Worden, V. Quitariano, and K. Pankow, 2005, *ShakeMap Manual: Technical Manual, Users Guide, and Software Guide* (Version 1.0  
302 ed.). United States Geological Survey, <http://pubs.usgs.gov/tm/2005/12A01/>.

303 Watt, J. T., R. W. Graymer, R. W. Simpson, D. A. Ponce, R. C. Jachens, G. A. Phelps, and C. M. Wentworth, 2007, A three-dimensional geologic  
304 model of the Hayward-Calaveras fault junction, *EOS Trans.*, v. 88, no. 52, S21A-0238.

305 Wentworth, C. M., G. R. Fisher, P. Levine, and R. C. Jachens, 1995, The surface of crystalline basement, Great Valley and Sierra Nevada,  
306 California: A digital map database, U.S. Geological Survey Open-File Report 95-96.

307 Wessel, P. and W. H. F. Smith, 1998, New, improved version of the generic mapping tools released, *EOS Transactions*, v. 79, p. 579.

308 Working Group on California Earthquake Probabilities, 2003, Earthquake probabilities in the San Francisco Bay Region: 2002–2031, U.S.  
309 Geological Survey Open-File Report 03-214.

310 Working Group on California Earthquake Probabilities, 2008, The uniform California earthquake rupture forecast, version 2 (UCERF 2), U.S.  
311 Geological Survey Open-File Report 2007-1437, <http://pubs.usgs.gov/of/2007/1437/> (last accessed 2/18/2009).

312 Yu, E. and P. Segall, 1996, Slip in the 1868 Hayward earthquake from the analysis of historical triangulation data, *Journal of Geophysical*  
313 *Research - Solid Earth*, v. 101, no. B7, p. 16101–16118.

314 Zhao, D., H. Kanamori, H. Negishi, and D. Wiens, 1996, Tomography of the source area of the 1995 Kobe earthquake: Evidence for fluids at the  
315 hypocenter?, *Science*, v. 274, no. 5294, p. 1891–1894.

316 Zoback, M. L., this volume.